

Article

# Sponge-Like Water De-/Ad-Sorption versus Solid-State Structural Transformation and Colour-Changing Behavior of an Entangled 3D Composite Supramolecular Architecture, $[\text{Ni}_4(\text{dpe})_4(\text{btc})_2(\text{Hbtc})(\text{H}_2\text{O})_9]\cdot 3\text{H}_2\text{O}$

Chih-Chieh Wang <sup>1,\*</sup>, Szu-Yu Ke <sup>1</sup>, Kuan-Ting Chen <sup>1</sup>, Ning-Kuei Sun <sup>1</sup>, Wei-Fang Liu <sup>1</sup>, Mei-Lin Ho <sup>1,\*</sup>, Bing-Jyun Lu <sup>1</sup>, Yi-Ting Hsieh <sup>1</sup>, Yu-Chun Chuang <sup>2</sup>, Gene-Hsiang Lee <sup>3</sup>, Shi-Yi Huang <sup>4</sup> and En-Che Yang <sup>4,\*</sup>

- <sup>1</sup> Department of Chemistry, Soochow University, Taipei 11102, Taiwan; sarah6017@yahoo.com.tw (S.-Y.K.); maxtw3336@gmail.com (K.-T.C.); coco830824@gmail.com (N.-K.S.); yvonne0123weifang@gmail.com (W.-F.L.); jason855180@gmail.com (B.-J.L.); ythsieh@gm.scu.edu.tw (Y.-T.H.)
- <sup>2</sup> National Synchrotron Radiation Research Center, Hsinchu 30076, Taiwan; chuang.yc@nsrrc.org.tw
- <sup>3</sup> Instrumentation Center, National Taiwan University, Taipei 10617, Taiwan; ghlee@ntu.edu.tw
- <sup>4</sup> Department of Chemistry, Fu Jen Catholic University, Xinbei 24205, Taiwan; s401192155@gmail.com
- \* Correspondence: ccwang@scu.edu.tw (C.-C.W.); meilin\_ho@scu.edu.tw (M.-L.H.); 071549@mail.fju.edu.tw (E.-C.Y.); Tel.: +886-2-2881-9471 (ext. 6828) (C.-C.W.)

Received: 26 August 2018; Accepted: 8 September 2018; Published: 11 September 2018



**Abstract:** An entangled composite compound,  $[\text{Ni}_4(\text{dpe})_4(\text{btc})_2(\text{Hbtc})(\text{H}_2\text{O})_9]\cdot 3\text{H}_2\text{O}$  (**1**), where  $\text{H}_3\text{btc}$  = 1,3,5-benzenetricarboxylic acid and dpe = 1,2-bis(4-pyridyl)ethane, has been synthesized and structurally characterized. Single-crystal structural determination reveals that compound **1** consists of four coordination polymers (CPs), with two two-dimensional (2D) (4,4) layered metal-organic frameworks (MOFs) of  $[\text{Ni}(\text{dpe})(\text{Hbtc})(\text{H}_2\text{O})]$  and  $[\text{Ni}(\text{dpe})(\text{btc})(\text{H}_2\text{O})]^-$  anion, and two one-dimensional (1D) polymeric chains of  $[\text{Ni}(\text{dpe})(\text{btc})(\text{H}_2\text{O})_3]^-$  anion and  $[\text{Ni}(\text{dpe})(\text{H}_2\text{O})_4]^{2+}$  cation, respectively. The three-dimensional (3D) supramolecular architecture of **1** is constructed via the inter-penetration of inter-digited, double-layered, 2D rectangle-grid MOFs by two 1D coordination polymeric chains, and tightly entangled together via the combination of inter-CPs  $\pi$ - $\pi$  stacking and hydrogen bonding interactions. The ad-/de-sorption isotherms of **1** for water displays a hysteresis profile with a maximum adsorption of 17.66 water molecules of per molecule unit at relative  $P/P_0 < 0.89$ . The reversible de-/re-hydration processes in **1** monitored by cyclic water de-/ad-sorption TG analysis and PXRD measurements evidence a sponge-like water de-/ad-sorption property associated with a thermal-induced solid-state structural transformation. The magnetic property of **1** suggests that the ferromagnetic coupling might refer to a stronger inter-Ni(II) interaction, which could be along the  $\text{btc}^{3-}$  or  $\text{Hbtc}^{2-}$  ligands; the antiferromagnetic coupling corresponding to the weaker inter-Ni(II) interactions, which could be the dpe ligands for the 2D framework.

**Keywords:** coordination polymer; metal-organic framework; supramolecular architecture; structural transformation; photoluminescence; magnetic property

## 1. Introduction

The study of 3D supramolecular architectures assembled via coordination polymers (CPs) [1] or metal organic frameworks (MOFs) [1,2] with various types of structural topologies is an important research topic, not only in terms of their structural diversity in the solid-state structural studies of

supramolecular chemistry [3–12], but also for their potential functional applications. A variety of supramolecular architectures have been obtained on the concepts of crystal engineering assembled by a large range of bonding forces, ranging from the classic M–L covalent bonds, to strong halogen interactions [13–21] or hydrogen bonds [22], to much weaker forces, such as weak hydrogen bonds [23,24] and  $\pi$ – $\pi$  stacking interactions of small aromatics [25–28]. In the field of supramolecular chemistry, entangled 3D supramolecular networks serve as an important subject via the assembly of various CPs, as seen in interpenetration, polycatenane, interdigitation, polythread, and other species [29–36]. Two or more CPs with different dimensionality—such as 1D plus 1D, 1D plus 2D, 2D plus 2D, and 2D plus 3D—within the crystal were found in the formation of their appealing interpenetrated or catenated 3D supramolecular networks [37–48]. Recently, a entangled 3D architecture composed of four CPs in a  $\text{Co}_4$  system with chemical formula  $[\text{Co}_4(\text{dpe})_4(\text{BTC})_2(\text{HBTC})(\text{H}_2\text{O})_{8.5}(\text{EtOH})_{0.5}] \cdot 3\text{H}_2\text{O}$  ( $\text{dpe}$  = 1,2-bis(4-pyridyl)ethane and  $\text{H}_3\text{BTC}$  = 1,3,5-benzenetricarboxylic acid) has been reported in our groups, which shows a composite combination of two 1D chains plus two 2D layers, extending to a 3D entangled supramolecular network [49]. Benzene-1,3,5-tricarboxylic acid ( $\text{H}_3\text{btc}$ ) is a rigid, planar molecule, and has been widely used as a bridging ligands on the construction of multi-dimensional MOFs in the form of its three benzene-1,3,5-triboxylate anions,  $\text{H}_2\text{btc}^-$ ,  $\text{Hbtc}^{2-}$ , and  $\text{btc}^{3-}$  [50–91]. Among these polymeric frameworks, the mixed-ligands Ni(II) CPs with 2D or 3D polymeric frameworks consisting of  $[\text{Ni}(\text{Hbtc})]$  [54–60] or  $[\text{Ni}_3(\text{btc})_2]$  [68,71–83] moieties as building units associated with nitrogen-based co-ligands have been investigated, and shown to possess interesting physical properties. However, composite 3D supramolecular architectures composed of two or more CPs are rare; only one example of  $[\text{Ni}(\text{H}_2\text{biim})_3][\text{Ni}(\text{btc})(\text{Hbim})] 2\text{H}_2\text{O}$  ( $\text{H}_2\text{biim}$  = 2,2'-biimidazole) is reported with its unique hydrogen-bonded pillared-layer 3D network being assembled by a 0D monomeric cation,  $[\text{Ni}(\text{H}_2\text{biim})_3]^{2+}$ , and a 2D anionic layers,  $[\text{Ni}(\text{btc})(\text{Hbim})]^{2-}$  [68]. In this work, we report on the exploration of a composite “four in one” supramolecular network,  $[\text{Ni}_4(\text{dpe})_4(\text{btc})_2(\text{Hbtc})(\text{H}_2\text{O})_9] \cdot 3\text{H}_2\text{O}$  (**1**), with  $[\text{Ni}(\text{Hbtc})]$  and  $[\text{Ni}(\text{btc})]$  moieties obtained by the reaction of Ni(II) nitrate with  $\text{dpe}$  and  $\text{H}_3\text{btc}$  ligands. This example represents a 3D supramolecular architecture composed of four crystallographically independent CPs, that is, two 2D (4,4) layered CPs,  $[\text{Ni}(\text{dpe})(\text{Hbtc})(\text{H}_2\text{O})]$  and  $[\text{Ni}(\text{dpe})(\text{btc})(\text{H}_2\text{O})]^-$ , and two 1D linear chain-like CPs,  $[\text{Ni}(\text{dpe})(\text{btc})(\text{H}_2\text{O})_3]^-$  and  $[\text{Ni}(\text{dpe})_2(\text{H}_2\text{O})_4]^{2+}$ , which are entangled together via the inter-penetration of the rectangular channels of inter-digitated 2D double-layered frameworks by 1D polymeric linear chains. The de-hydrated species **1**, after controlled heating at 240 °C, shows remarkable thermal-induced colour-changing behavior and reversibility to yield a re-hydrated structure when exposed to water vapor at 30 °C, indicating a sponge-like water de-/ad-sorption behavior and solid-state structural transformation.

## 2. Materials and Methods

### 2.1. Materials and Physical Techniques

General: All chemicals were of reagent grade and were used as commercially obtained without further purification. Elementary analyses (carbon, hydrogen and nitrogen) were performed using a Perkin-Elmer 2400 elemental analyzer (PerkinElmer, Taipei, Taiwan). IR spectra were recorded on a Nicolet Fourier Transform IR MAGNA-IR 500 spectrometer (Thermo Fisher Scientific, Waltham, MA, USA) in the range of 500–4000  $\text{cm}^{-1}$  using the KBr disc technique. Diffuse reflectance UV-vis spectra of **1** were obtained with a HITACHI U-4100 spectrophotometer equipped with an integrating sphere accessory ( $\text{Al}_2\text{O}_3$  was used as a reference). Thermogravimetric analysis (TGA) of compound **1** was performed on a computer-controlled Perkin-Elmer 7 Series/UNIX TGA7 analyzer (PerkinElmer, Taipei, Taiwan). The adsorption isotherm of  $\text{H}_2\text{O}$  (298 K) was measured in the gaseous state by using BELSORP-max volumetric adsorption equipment from BEL, Osaka, Japan. In the sample cell ( $\sim 1.8 \text{ cm}^3$ ) maintained at  $T \pm 0.03 \text{ K}$  was placed the adsorbent sample ( $\sim 100$ – $150 \text{ mg}$ ), which has been prepared at 180 °C for **1** and  $10^{-2} \text{ Pa}$  for about 24 h prior to measurement of the isotherm. The adsorbate was placed into the sample cell; the change of pressure was then monitored, and the degree of

adsorption was determined by the decrease of pressure at equilibrium state. All operations were automatically computer-controlled. Single-phased powder samples were loaded into alumina pans and heated with a ramp rate of 5 °C/min from room temperature to 800 °C under a nitrogen atmosphere. Diffuse reflectance UV-vis spectra of **1** were obtained with a HITACHI U-3900H spectrophotometer (Hitachi High Technologies America, Inc., Schaumburg, IL, USA) equipped with an integrating sphere accessory (Al<sub>2</sub>O<sub>3</sub> was used as a reference). The temperature-dependent magnetic susceptibility was measured on the SQUID system with 2 kOe external magnetic field.

## 2.2. Synthesis of [Ni<sub>4</sub>(dpe)<sub>4</sub>(btc)<sub>2</sub>(Hbtc)(H<sub>2</sub>O)<sub>9</sub>] 3H<sub>2</sub>O (**1**)

A solution of 1,3,5-benzenetricarboxylic acid (H<sub>3</sub>btc, 4.2 mg, 0.02 mmol) and 1,2-bis(4-pyridyl)ethane (dpe, 5.2 mg, 0.03 mmol) in mixed solvents of distilled water and EtOH (1:1, *v/v*) (9 mL) was added to a solution of Ni(NO<sub>3</sub>)<sub>2</sub>·6H<sub>2</sub>O (8.72 mg, 0.03 mmol) in mixed solvents of distilled water and EtOH (1:1, *v/v*) (3 mL) to give a pale-green solution which was left to stand at 80 °C in the oven for 72 h, and then at RT for several days. Light-blue plate-shaped crystals were collected by filtration and washed several times with distilled water, and then dried in air; yields of 40.3% were obtained. Elemental Analysis Calculated (Anal. Calc.) or C<sub>75</sub>H<sub>82</sub>N<sub>8</sub>Ni<sub>4</sub>O<sub>30</sub> (M<sub>w</sub> = 1810.33): C 49.76, N 6.19, H 4.57. Found: C 49.90, N 6.15, H 4.23. IR (KBr pellet):  $\nu$  = 3468 (w), 3461 (w), 3037 (w), 1698 (s), 1635 (m), 1618 (m), 1559 (vs), 1427 (m), 1236 (s), 766 (m) cm<sup>-1</sup>.

## 2.3. Crystallographic Data Collection and Refinements

Single-crystal structural analysis for compound **1** was performed on a Siemens SMART diffractometer with a CCD detector with Mo radiation ( $\lambda$  = 0.71073 Å) at 100 K. A preliminary orientation matrix and unit cell parameters were determined from 3 runs of 15 frames each, with each frame corresponding to a 0.3° scan over 10 s, followed by spot integration and least-squares refinement. For each structure, data were measured using  $\omega$  scans of 0.3° per frame for 20 s until a complete hemisphere had been collected. Cell parameters were retrieved using SMART [92] software and refined with SAINT [93] on all of the observed reflections. Data reduction was performed with the SAINT [94] software and corrected for Lorentz and polarization effects. Absorption corrections were applied with the program SADABS [94]. Direct phase determination and subsequent difference Fourier map synthesis yielded the positions of all non-hydrogen atoms, which were subjected to anisotropic refinements. All hydrogen atoms were generated geometrically (C–H = 0.93 (C<sub>sp2</sub>–H) or 0.97 (C<sub>sp3</sub>–H) Å), with the exception of those of the coordinated water molecules, which were located in the difference Fourier map with the corresponding positions and isotropic displacement parameters being refined. The final full-matrix, least-squares refinement on  $F^2$  was applied for all of the observed reflections ( $I > 2\sigma(I)$ ). All calculations were performed using the SHELXTL-PC V 5.03 software package (Siemens Analytical Instruments Division, Madison, WI, USA) [95]. Crystal data and details of the data collection and structure refinements for **1** are summarized in Table 1. CCDC-1498095 for **1** contains the supplementary crystallographic data for this paper. These data can be obtained free of charge at [www.ccdc.cam.ac.uk/conts/retrieving.html](http://www.ccdc.cam.ac.uk/conts/retrieving.html) or from the Cambridge Crystallographic Data Centre, 12, Union Road, Cambridge CB2 1EZ, UK; fax: (internat.) +44-1223/336-033; email: [deposit@ccdc.cam.ac.uk](mailto:deposit@ccdc.cam.ac.uk).

**Table 1.** Crystal data and refinement details of compound **1**.

Empirical Formula	C <sub>75</sub> H <sub>82</sub> N <sub>8</sub> Ni <sub>4</sub> O <sub>30</sub>	Formula Mass (g mol <sup>-1</sup> )	1810.33
crystal system	Orthorhombic	space group	Pna2 <sub>1</sub>
<i>a</i> /Å	20.3669(9)	$\alpha$ (°)	90
<i>b</i> /Å	13.6680(6)	$\beta$ (°)	90
<i>c</i> /Å	27.1571(12)	$\gamma$ (°)	90
<i>V</i> /Å <sup>3</sup>	7559.9(6)	Z	4
<i>D</i> <sub>calcd</sub> (g cm <sup>-3</sup> )	1.591	$\theta$ range (deg.)	1.49–27.50
$\mu$ /mm <sup>-1</sup>	1.075	<i>T</i> (K)	150(2)
total no. of data collected	56,835	no. of unique data	13,812
<i>R</i> <sub>1</sub> , <i>wR</i> <sub>2</sub> <sup>1</sup> ( <i>I</i> > 2 $\sigma$ ( <i>I</i> ))	0.0636, 0.1226	<i>R</i> <sub>1</sub> , <i>wR</i> <sub>2</sub> <sup>1</sup> (all data)	0.0856, 0.1324
GOF <sup>2</sup>	1.072	refine params	1050

$$^1 R_1 = \sum ||F_o - F_c| | / \sum |F_o|; wR_2(F^2) = [\sum w|F_o^2 - F_c^2|^2 / \sum w(F_o^4)]^{1/2}; ^2 GOF = \{\sum [w|F_o^2 - F_c^2|^2] / (n - p)\}^{1/2}.$$

#### 2.4. In Situ X-ray Powder Diffraction

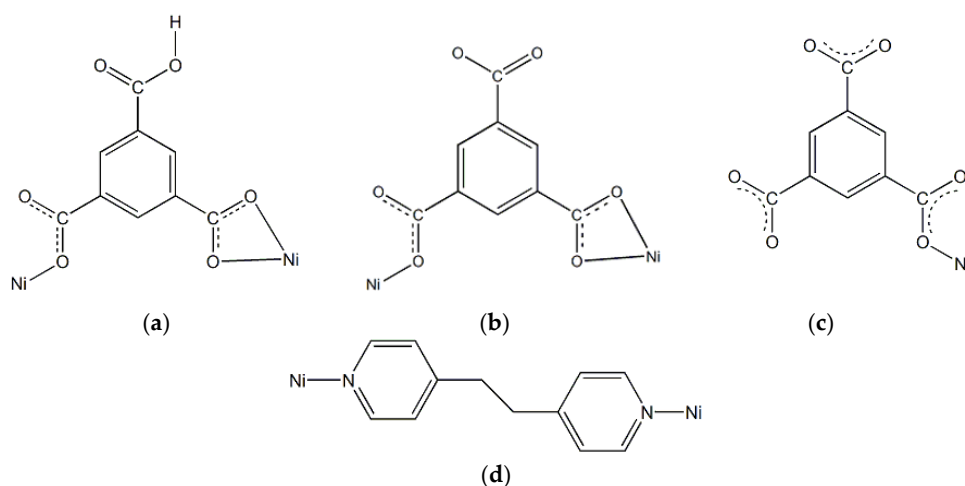
The synchrotron powder X-ray diffraction data of **1** were collected at the BL01C2 beamline at the National Synchrotron Radiation Research Center (NSRRC) in Taiwan. The wavelength of the incident X-rays is 1.03321 Å and the diffraction patterns were recorded with a Mar345 imaging plate detector placed approximately 331 mm from sample positions. The one-dimensional powder diffraction profile was converted with program FIT2D [96] and cake-type integration, where the diffraction angles were calibrated according to Bragg positions of Ag-Benhenate and Si powder (SRM640c) standards. In-situ temperature dependent experiment for **1** was performed from 28 to 300 °C, with a heating rate 10 °C/min. The powder sample was packed in a glass capillary (0.3 mm diameter) and heated in a stream of hot air; each pattern was exposed for about 1.2 min. The capillary of de-hydrated sample was immersed in water for one hour, then the powder pattern was measured again.

### 3. Results and Discussion

#### 3.1. Synthesis and Structural Description of [Ni<sub>4</sub>(dpe)<sub>4</sub>(btc)<sub>2</sub>(Hbtc)(H<sub>2</sub>O)<sub>9</sub>].3H<sub>2</sub>O (**1**)

Compound **1** was synthesized by the reactions of the mixing of nickel(II) nitrate, dpe, and H<sub>3</sub>btc in ethanol/water solution with molar ratios of 3:3:2 standing in the oven at 80 °C, resulting in the formation of light-blue crystals of **1**, formulated as [Ni<sub>4</sub>(dpe)<sub>4</sub>(btc)<sub>2</sub>(Hbtc)(H<sub>2</sub>O)<sub>9</sub>].3H<sub>2</sub>O, which are suitable for X-ray diffraction analysis. Structural determination reveals that the crystal structure of **1** show the presence of four crystallographically independent polymeric structures entangled together: containing two 2D layered CPs of neutral [Ni(dpe)(Hbtc)(H<sub>2</sub>O)] **A**, anionic [Ni(dpe)(btc)(H<sub>2</sub>O)]<sup>-</sup> **B**, two 1D polymeric chain-like CPs of anionic [Ni(dpe)(btc)(H<sub>2</sub>O)<sub>3</sub>]<sup>-</sup> **C**, and cationic [Ni(dpe)(H<sub>2</sub>O)<sub>4</sub>]<sup>2+</sup> **D**, respectively. In total, **1** can be formulated as [Ni(dpe)(Hbtc)(H<sub>2</sub>O)][Ni(dpe)(btc)(H<sub>2</sub>O)][Ni(dpe)(btc)(H<sub>2</sub>O)<sub>3</sub>][Ni(dpe)(H<sub>2</sub>O)<sub>4</sub>].3H<sub>2</sub>O; all the oxidation states of four independent nickel centers are 2+. The coordination environments of Ni(II) ions in **A** and **B** are both six-coordinate with a distorted octahedral geometry, (shown in Figure S1a,b in the supplementary materials, respectively), bonded to two nitrogen atoms of two *anti*-dpe, and four oxygen atoms of one water molecule and two Hbtc<sup>2-</sup> ligands in **A**, and two btc<sup>3-</sup> ligands in **B**, respectively. The related bond-lengths around the Ni(II) ions are listed in Table S1 (Supplementary Materials). The Hbtc<sup>2-</sup> in **A** and btc<sup>3-</sup> in **B** both act as the bridge ligands with chelating/monodentate coordination mode (Scheme 1a,b) connecting the Ni(II) ions to form linear chains. Adjacent chains are then mutually connected via the bridges between the Ni(II) ions and dpe ligand with *bis*-monodentate coordination mode (Scheme 1d), to generate 2D layered MOFs (Figure 1a) with a 4<sup>4</sup> structural topology by using rectangle-grid as the basic building block. The rectangle-grid dimensions are 10.263 × 13.668 Å (Figure 1a, bottom, left) via the bridges of Hbtc<sup>2-</sup> and *anti*-dpe in **A**, and 10.184 × 13.668 Å (Figure 1a, bottom, right) via the bridges of btc<sup>3-</sup> and *anti*-dpe in **B**, respectively. Moreover, **A** and **B** are mutually inter-digitated into each other along the direction of the uncoordinated carboxylate groups of the lateral Hbtc<sup>2-</sup> and btc<sup>3-</sup> ligands, respectively, to fabricate a 2D double-layered {**AB**}

network (Figure 1a, bottom, middle), resulting in the formation of inner rectangular channels with dimensions of ca.  $6.834 \times 10.223 \text{ \AA}$ . The lateral  $\text{Hbtc}^{2-}$  in **A** and  $\text{btc}^{3-}$  in **B** are oriented vertically up and down, respectively, into the double-layered network as the walls of the channels. The coordination environments of Ni(II) ions in **C** and **D** are both six-coordinate (shown in Figure S1c,d deposited in the supplementary materials), in which the Ni(II) ion in **C** has a distorted  $\{\text{NiN}_2\text{O}_4\}$  octahedral geometry (Figure S1c, Supplementary Materials) which is bonded to two nitrogen atoms of two *anti*-dpe ligands with *bis*-monodentate coordination mode (Scheme 1d, Supplementary Materials), four oxygen atoms of one  $\text{btc}^{3-}$  ligand with monodentate coordination mode (Scheme 1c, Supplementary Materials), and three water molecules, while the Ni(II) ion in **D** also has a distorted  $\{\text{NiN}_2\text{O}_4\}$  octahedral geometry (Figure S1d, Supplementary Materials) bonded to two nitrogen atoms of two *anti*-dpe ligands with *bis*-monodentate coordination mode (Scheme 1d, Supplementary Materials), and four oxygen atoms of four water molecules. The related bond lengths around the Ni(II) ions are listed in Table S1. Both **C** and **D** are 1D polymeric linear chains via the connectivity between the Ni(II) ions, and *anti*-dpe ligands extending along the *c* axis, as shown in Figure 1b.



**Scheme 1.** (a) chelating/monodentate coordination mode of  $\text{Hbtc}^{2-}$  in **A**; (b) chelating/monodentate coordination mode of  $\text{btc}^{3-}$  in **B**; (c) monodentate coordination mode of  $\text{btc}^{3-}$  in **C**; and (d) *bis*-monodentate coordination mode of *dpe*.

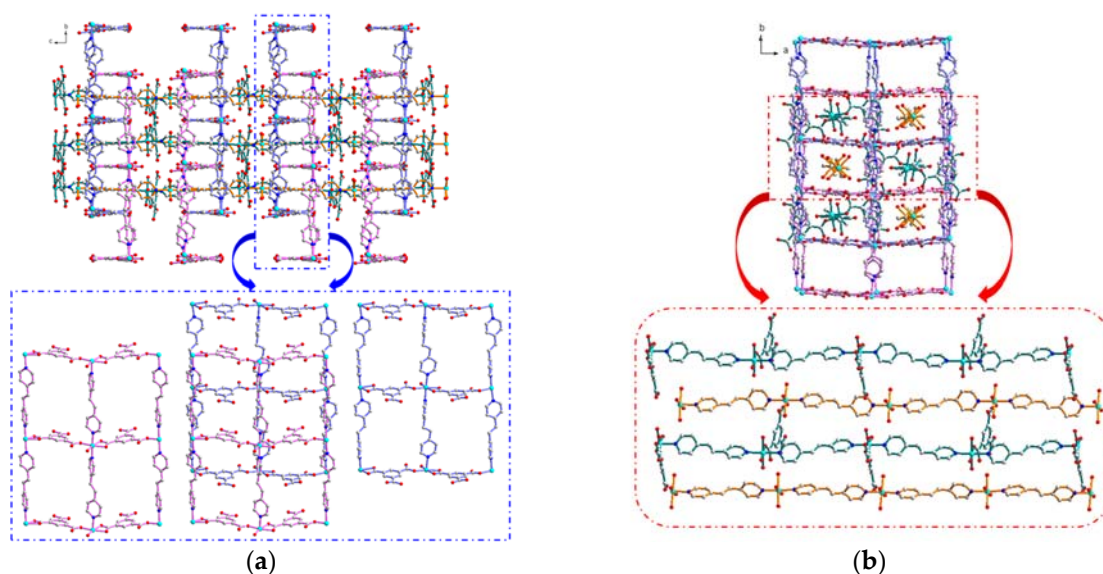


**Figure 1.** Cont.



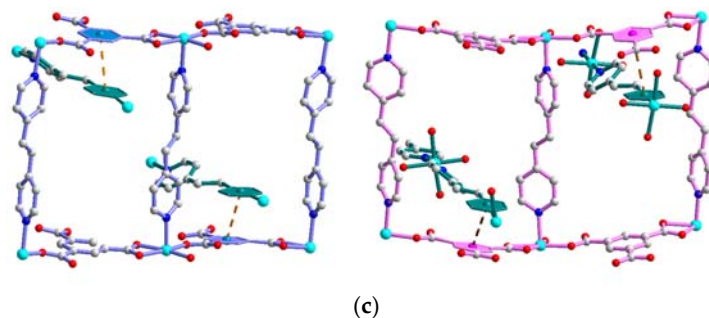


**Figure 1.** (a) Up: 3D supramolecular entangled architecture in **1** showing the interpenetration of two 1D chains (**C** and **D**) into the rectangular channels formed by 2D double-layered network (**A** plus **B**) viewing along the *a* axis. Bottom, middle: 2D double-layers of **A** plus **B** viewing along the *c* axis; right: 2D rectangle-grid layer of **A**, with grid-dimensions of  $10.263 \times 13.668$  Å; left: 2D rectangle-grid layer of **B**, with grid-dimensions of  $10.184 \times 13.668$  Å, (b) up: 3D supramolecular entangled architecture in **1** viewing along the *c* axis showing the interpenetration of two 1D chains (**C** and **D**) in an alternate array. Bottom: two 1D linear chains of **C**, and **D**, (c)  $\pi$ - $\pi$  interactions between the pyridine rings of *anti*-dpe ligands and the benzene rings of the  $\text{Hbtc}^{2-}$  or  $\text{btc}^{3-}$  ligands.

The most remarkable and interesting structural feature of **1** is the 3D tightly-entangled supramolecular architecture, which is composed of a 2D  $\{[\text{Ni}(\text{dpe})(\text{Hbtc})(\text{H}_2\text{O})]^- [\text{Ni}(\text{dpe})(\text{btc})(\text{H}_2\text{O})]\}$ , (**AB**) double-layers and two 1D  $[\text{Ni}(\text{dpe})(\text{btc})(\text{H}_2\text{O})_3]^-$  (**C**) and  $[\text{Ni}(\text{dpe})_2(\text{H}_2\text{O})_4]^{2+}$  (**D**) polymeric chains, as shown in Figure 1a,b. First of all, adjacent double-layered frameworks of {**A** plus **B**} are arranged parallel in an **{AB}{BA}{AB}{BA}** ... manner (Figure 1a, up) along the *c* axis, generating 1D rectangular channels (Figure 1b, up). These channels are then fully occupied by the 1D polymeric linear chains of **C** and **D** in an alternate **CD** sequence to complete its unique 3D supramolecular array. To the best of our knowledge, this is the first 3D entangled  $\text{Ni}_4$  supramolecular network constructed via the composite combination of two 1D chain-like CPs plus two 2D layered CPs by inter-digitation and inter-penetration. Most importantly, the subtle combination of hydrogen-bonding and  $\pi \dots \pi$  stacking interactions among the four CPs both play significant roles in the construction of its 3D tightly entangled architecture. Firstly, 4 sets of intra-CP O-H ... O type hydrogen bonds with the O ... O distances in the ranges of 2.518(9)–2.861(9) Å, and 11 sets of inter-CPs O-H ... O type hydrogen bonds with the O ... O distances in the ranges of 2.591(9)–2.830(9) Å between the coordinated water molecules and the oxygen atoms of  $\text{Hbtc}^{2-}$  or  $\text{btc}^{3-}$  ligands among the four CPs, provide extra energy on the stabilization of the entangled architecture. Furthermore, three solvated water molecules intercalated in the vacant pores of the 3D supramolecular architecture are reinforced by 9 sets of intermolecular O-H ... O type hydrogen bonding interactions between the solvated water molecules and the oxygen atoms of coordinated water molecules,  $\text{Hbtc}^{2-}$  and  $\text{btc}^{3-}$  ligands, with O ... O distances in the range of 2.643–2.941 Å. The mutually linkage of intra-CP and inter-CP hydrogen bonding interactions among four CPs and solvated water molecules not only stabilize the entangled 3D network, but also provide the possible pathways for the reversible water de-/ad-sorption behavior during thermally de-/re-hydration processes, which will be discussed in the following section. The common hydrogen-bonding distances and angles in **1** are summarized in Table S2 (Supplementary Materials). Furthermore,  $\pi$ - $\pi$  stacking interactions between the pyridine rings of *anti*-dpe ligands and the benzene rings of the  $\text{Hbtc}^{2-}$  or  $\text{btc}^{3-}$  ligands, with the ring centroid distances in the range of 3.498–3.995 Å, provide the extra stabilization energy on the construction of the 3D entangled assembly of **1**. A schematic representation of two  $\pi$ - $\pi$  interactions with shorter ring centroid distances is shown in Figure 1c. The related inter-planar parameters are listed in Table S3 (deposited in Supplementary Materials). The surface morphology of the crystals of **1**, through the SEM images in Figure 2a, shows rod-shaped formations. The enlarged images at different positions (Figure 2b,c) reveal that **1** was stacked up with numerous crack-free, 2D layers; each layer is completely made up of small crystals.

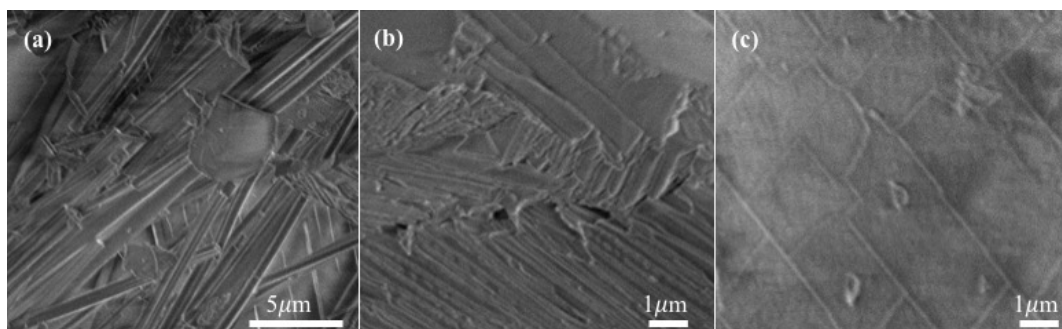


**Figure 2.** SEM images of crystals **1** with different magnifications (a) the global view; (b,c) enlarged images at different positions. The acceleration voltage is 2 kV.

### 3.2. Thermal Stability of **1** by TG Analysis and In Situ Powder X-ray Diffraction Analyses

A thermogravimetric analysis (TGA) of **1** was performed to assess the thermal stability on the 3D entangled network as a function of temperature. During the heating process, the TG analysis (Figure 3a) revealed that **1** underwent a two-steps weight loss of total 12.4%, which corresponded to the loss of 3 solvated water molecules (calc 3.0%), occurring in the range of approximately 31–109 °C for the first step, and 9 coordinated water molecules (calc 9.0%), occurring in the range of approximately 109–178 °C for the second step. In the temperature range of approximately 178–310 °C, de-hydrated **1** was stable without any weight loss. On further heating, these samples decomposed at approximate 310 °C. In order to gain structural variation in depth upon de-hydration of water molecules, in situ synchrotron X-ray powder diffraction patterns of **1** were collected continuously from 25 to 480 °C; the results at some specific temperatures are shown in Figure 3b. The powder pattern of fresh sample at RT matches well with the simulated pattern based on the single crystal structure. As the temperature increases, a phase transition occurred at 210 °C, and converted to a meta-stable phase at 240 °C. It is unfortunate that, due to the poor long range ordering of PXRD data, the unit cell of de-hydrated form **1** could not be determined directly using synchrotron PXRD diffraction data.

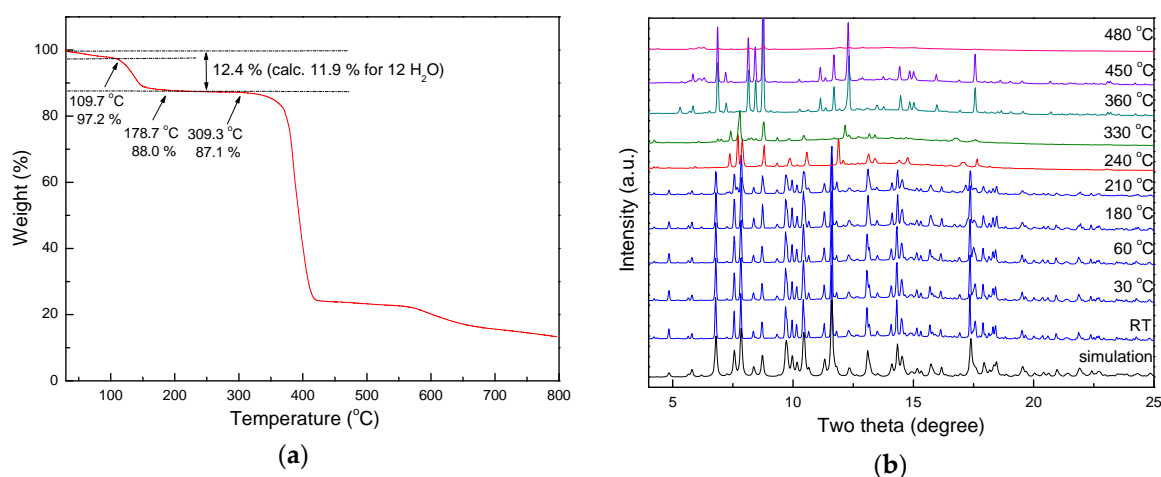


**Figure 3.** (a) Thermogravimetric (TG) analysis of **1**; (b) In-situ PXRD patterns of **1** at different temperatures, and simulated PXRD pattern from single-crystal X-ray diffraction data.

### 3.3. Reversible Water De-/Ad-Sorption Behavior Accompanying with Morphological Changes during the Thermal De-/Re-Hydration Processes

In order to verify the reversibility of water de-/ad-sorption property of **1** during the re-/de-hydration processes, cyclic TG measurements were taken under water vapor by thermal treatment, as shown in Figure 4a. The de-hydrated **1** after the de-hydration process by the thermal

treatment (up to 200 °C) shows a 10.7% weight loss, corresponding to 10.8 H<sub>2</sub>O molecules. The water molecules can then be re-adsorbed by exposing the de-hydrated **1** to water vapor, forming a re-hydrated crystal with a weight increase of 13.4%, corresponding to approximate 13.5 water molecules when the sample cooled down to room temperature. Such heating (up to 200 °C) and cooling (down to RT) procedures were repeated for five cycles, as shown in Figure 4a, with almost the same weight-increase/weight-decrease percentages (12.4%~13.5%); this was in order to demonstrate the stable reversibility of the thermal re-/de-hydration processes. This result evidences that **1** adopts a reversible water de-/ad-sorption sponge-like property between de-hydrated and re-hydrated forms, driven by thermal re-/de-hydration treatments. It is also important to note that this water de-/ad-sorption sponge-like property was accompanied by morphological changes. The simultaneous and gradual colour change of the crystal during the de-/re-hydration processes was followed by optical microscopy (Figure 4b). A Well-formed blue crystal of **1** was obtained as a plate-shaped sheet, shown in Figure 4b (left, bottom), at RT. **1** undergoes reversible colour-changing behavior when the temperature rises, with the colour gradually shifting from blue to brown-green (Figure 4b, left side from bottom to top). As the temperature was raised from RT to 50, 100, 140, 200 and 250 °C, the colour of dried crystal gradually became deeper than that at RT, and many chaps with random cracks on the crystal surface were observed. The obvious colour change from blue to brown-green took place from 140 to 200 °C upon the loss of solvated and coordinated water molecules, respectively. Furthermore, the brown-green de-hydrated crystal was slowly turned back to a blue, re-hydrated one (Figure 4b, right side from top to bottom) as the temperature decreased from 250 °C to RT, indicating the slow re-hydration procedure from water vapor in the air. Finally, the brown-green de-solvated sample gradually returned to its original blue as the crystal was exposed to air at RT and left to stand for more than one day. However, the transparency of the re-hydrated crystal was not as high as that of the fresh crystal. In order to understand the interactions of guest and coordinated water molecules within the host framework, the water vapor sorption performance of de-hydrated **1** was also studied at 298 K (Figure 4c). For water vapor adsorption, an increase in the amount of adsorbed vapor was found at  $0 < \text{relative } P/P_0 < 0.89$ , with maximum adsorption of 17.66 water molecules of per molecule unit at relative  $P/P_0 < 0.89$ , indicating that nine coordinated water molecules, and more than three guest water molecules (found in the crystal structure) were absorbed. Such an observation is in agreement with the result in the cyclic TG measurements (Figure 4a). It is worth noting that the desorption curve did not trace the adsorption curve any longer, which exhibited a large hysteresis with the 9.73 water molecules of per molecule unit at relative  $P/P_0 = 0.05$ , nearly corresponding to 9 coordinated water molecules found in the crystal structure. This result reveals that the water molecules are strongly interacted with the 1D or 2D CPs, not only through the coordination with Ni(II) ions, but also through hydrogen bonding interactions; therefore, desorption was rendered difficult, resulting in a hysteresis profile. The water adsorption had dynamic adsorption property, wherein the de-hydrated host framework changed according to the water molecules entering. Further study of the sponge-like water de-/adsorption property correlated with the thermal-induced solid-state structural transformation and UV-vis absorption properties. Other properties of **1** will be discussed in the next sections.



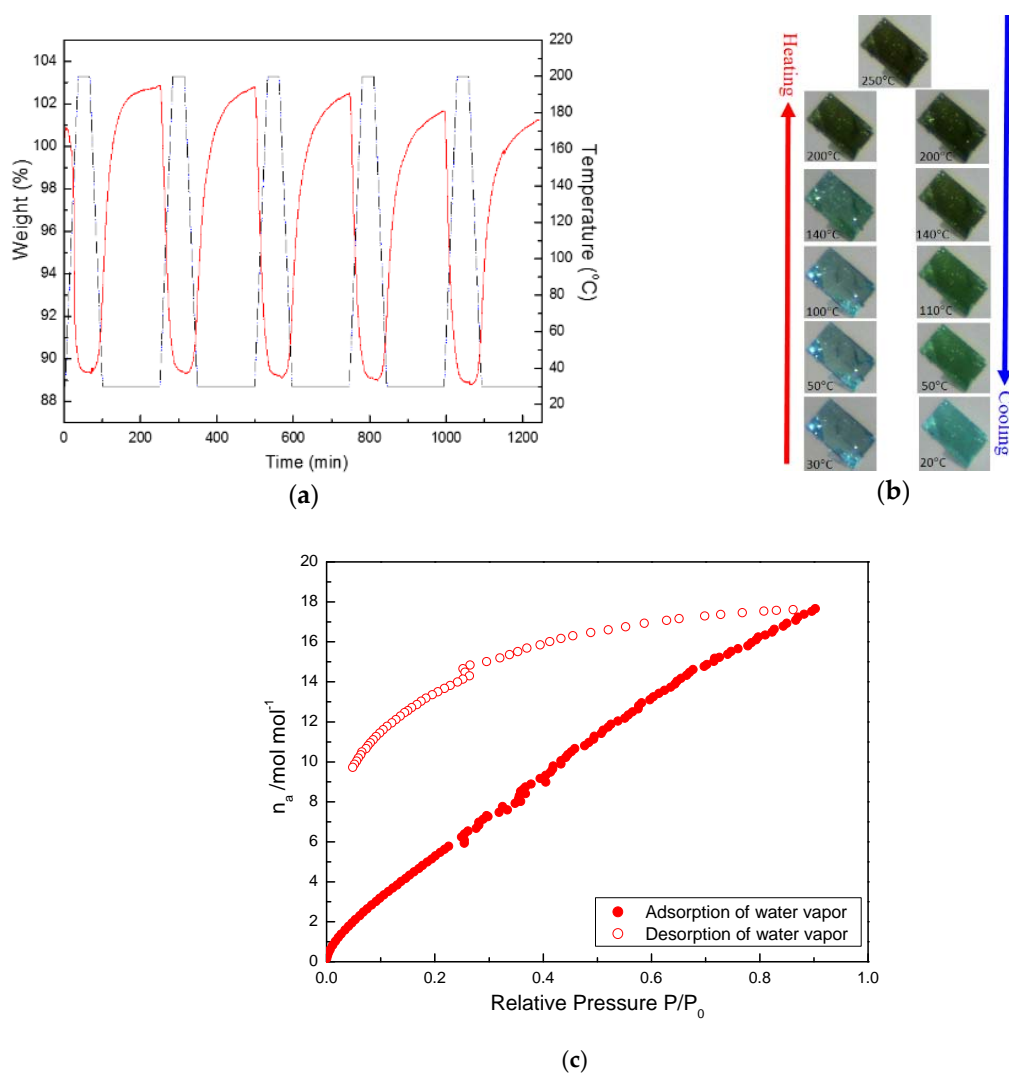


**Figure 4.** (a) TG measurements of cyclic de-/re-hydration processes for **1** were repeated four times. Solid red line: the variation of weight loss with time; black dash-dot line: the variation of temperature with time. (b) Photographs of plate-shaped crystal **1** at different temperatures. (c) Water Vapor ad-/desorption isotherms at 298 K for **1**.

#### 3.4. Solid-State Structural Transformation by Thermal De-/Re-Hydration Processes

The most promising feature of crystal **1** is that it adopts sponge-like reversible water de-/ad-sorption behavior by thermal de-/re-hydration processes, which has been identified by cyclic TG and morphological measurements. Furthermore, the correlation between the water de-/ad-sorption sponge-like property and the dynamic solid-state structural transformation during the de-/re-hydration processes is also important, and worthy of further study by PXRD analysis. As shown in Figure 5c,e, when the de-hydrated samples of **1** at 240 °C is cooled down to RT and exposed to water (i.e., the de-hydrated sample is placed in a glass capillary, beside a beaker filled with water or immersed in the beaker), it re-absorbs the water molecules. The PXRD pattern of the re-hydrated species that immersed into the water solution (Figure 5e) is not matched so well to that of the freshly synthesized samples (Figure 5b), which indicates that the structure of re-hydrated species may be slightly different or incompletely transferred to the original structure **1**, and is re-established as a new re-hydrated form. The results indicates that **1** may undergoes a reversible dynamic solid-state structural transformation between the de-hydrated form and a new re-hydrated form, and that the re-hydrated structure of **1** may be similar but slightly different to its original structure, which has

been demonstrated from the water ad-/de-sorption isotherms (shown in Figure 4c), with more than three guest water molecules being absorbed. Owing to the structures of the de-hydrated form in the high temperature phase, and rehydrated species at RT, the structures cannot be determined directly by PXRD data; therefore, the structural transformation mechanism for the thermal dehydration processes is not clear. However, the reversibly dynamic solid-state structural transformation may be attributed to the significant hydrogen bonding interactions among the coordinated, solvated water molecules and oxygen atoms of the Hbtc<sup>2-</sup> and btc<sup>3-</sup> ligands in four CPs. The relatively easy release of the coordinated water molecules under a gentle thermal process is indeed made possible by a carboxylate-assisted process; a structural drawing illustrating the proximity of carboxylate fragments (Hbtc<sup>2-</sup> and btc<sup>3-</sup>) and the coordinated water molecules among four CPs is shown in Figure 6. A possible route for the reversible structural transformation route between de-hydrated form and re-hydrated form could be that the removal of the coordinated water molecules creates open sites of Ni(II) centers for the approach of neighboring oxygen atoms of the Hbtc<sup>2-</sup> and btc<sup>3-</sup> ligands, which are also oriented towards the coordination water molecules of neighboring units via O–H . . . O hydrogen bonds [97]. These contacts shorten in the course of the solid-state reaction, and turn into bonds with Ni(II) atoms after the removal of the water molecules to generate the de-hydrated form, and then re-absorb to form the re-hydrated form after the de-hydrated sample is exposed to water vapor.

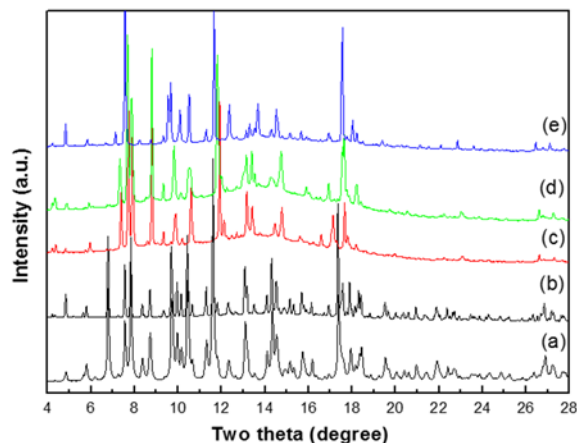


**Figure 5.** PXRD patterns of (a) simulation of **1** from single-crystal X-ray diffraction data; (b) fresh samples of **1** at RT; (c) De-hydrated samples of **1** at 240 °C; (d) the de-hydrated samples **1** exposed to the air at RT; (e) the re-hydrated samples obtained by the de-hydrated samples **1** immersed in the water solution.

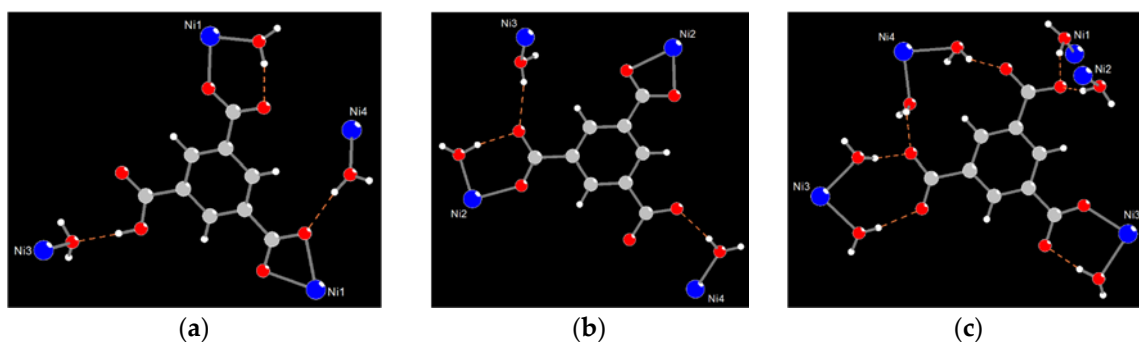


**Figure 6.** The proximity of intra- and inter-molecular hydrogen bonds between the carboxylate fragments of (a) Hbtc<sup>2-</sup> fragment in **A**; (b) btc<sup>3-</sup> fragment in **B**; (c) btc<sup>3-</sup> fragment in **C** respectively, and the coordinated water molecules.

### 3.5. Colour-Changing Behavior and UV-vis Absorption Property of De-/Re-Hydration for Crystal 1

Finally, as shown in Figure 7, the crystal **1** shows two bands at 387 and 645 nm, which may be attributed to the  ${}^3A_{2g}(F) \rightarrow {}^3T_{1g}(P)$  and  ${}^3A_{2g}(F) \rightarrow {}^3T_{1g}(F)$  electronic transitions, respectively; this indicates an octahedral geometry around the Ni(II) center [98–100]. These transitions are consistent with the crystal structure of **1**. To further observe the temperature-dependent change processes of the crystal, in situ heating/cooling UV-vis absorption spectroscopy was used to characterize the change of these two transitions. As depicted in Figure 7, upon heating from RT to 300 °C, the intensity of these two bands tends to increase, accompanied by the gradual red-shift of the bands. This result indicates that the coordination environments around the Ni(II) have been changed upon heating, and hence, result in the energy change of d-d transitions. In particular, after heating to 170 °C, the absorbance at 387 nm had a maximum shift with 8 nm to 395 nm, which can be attributed to the loss of the coordination waters around the Ni(II). This result is in accordance with that of the TG and PXRD analyses (vide supra). Furthermore, as the temperature decreased from 200 °C to RT after one hour, the absorption shifted back to the 387 nm (see dash line), which is the same position at RT, and accompanied the intensity enhancement. This indicates that the water has come back to the coordination center during the rehydration process. The rehydration crystal at RT has a more intense absorption intensity than that of the original crystal, which may be attributed to the fact that the rehydration structure is slightly different compared to that of **1** (vide supra), and hence, leads to a different d-orbital energy state change.

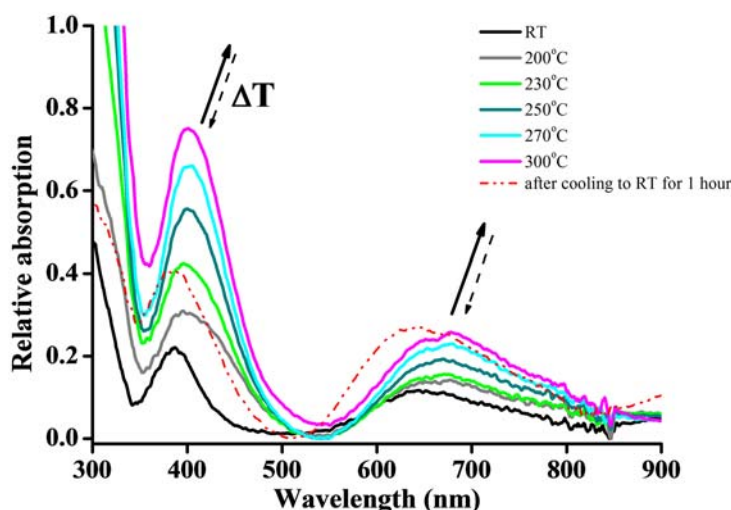


**Figure 7.** The UV-vis diffuse reflectance spectra of **1** upon heating and cooling from RT to 300 °C.

### 3.6. Magnetic Property of **1**

The magnetic properties of compound **1** were explored by dc magnetic susceptibility measurements. The experiment was performed on a polycrystalline sample under a 2000 G magnetic field in the temperature range of 2 to 300 K. Figure 8 illustrates the  $\chi_M T$  vs.  $T$  plot, with the experimental data as the black square points. It can be seen that the  $\chi_M T$  value is about 4.5 cm<sup>3</sup> K/mol at 300 K, which corresponds to four uncoupled Ni(II) ions with  $g = 2.13$ . Upon cooling, the  $\chi_M T$  values slightly go up and reach the maximum 4.72 cm<sup>3</sup> K/mol at 45 K. The behavior of the increase of the  $\chi_M T$  values on cooling indicates a weak ferromagnetic coupling dominant on one direction of the 2-dimensional net structure. With continued cooling, the  $\chi_M T$  values slowly decrease to 4.0 cm<sup>3</sup> K/mol at 5 K, and drop abruptly to 2.76 cm<sup>3</sup> K/mol at 2 K. This behavior strongly suggests that an antiferromagnetic coupling interaction is in the other direction of the 2-dimensional network. To simulate this majorly 2-dimensional network of Ni(II) ions, a 2-D Ising-like coupling scheme was employed.

$$H = -\sum 2J_1 S(i,j) \cdot S(i+1,j) - \sum 2J_2 S(i,j) \cdot S(i,j+1) \quad (1)$$

The simulation was done by applying Equation (1) to the program MAGPACK [101,102]. The result of the simulation, based on Equation (1), is presented as red solid line in Figure 8, which gives  $J_1 = +0.4$  K,  $J_2 = -0.34$  K and  $g = 2.15$ . It is clear that the strength of ferromagnetic coupling is stronger than the antiferromagnetic coupling, so that the  $\chi_M T$  values increase on cooling when the temperatures are high, but drop deeply at very low temperatures ( $\sim 2$  K). Judging from the structure, there seems to be two pathways that can conduct magnetic coupling, i.e.,  $\text{btc}^{3-}/\text{Hbtc}^{2-}$  and dpe ligands. From the literature, most btc ligand binding Ni(II) ions are antiferromagnetic coupling [103,104], whereas the dpe ligand, due to its large size, usually ignores the magnetic exchange coupling [105]. As the ferromagnetic coupling, in our case, is stronger than the antiferromagnetic one, it seems to be unreasonable to suggest that the ferromagnetic coupling came purely from the dpe pathway. Therefore, we suggest the antiferromagnetic coupling may be the result of  $\text{btc}^{3-}/\text{Hbtc}^{2-}$  bridging; however, the source of the ferromagnetic coupling still remains unclear.

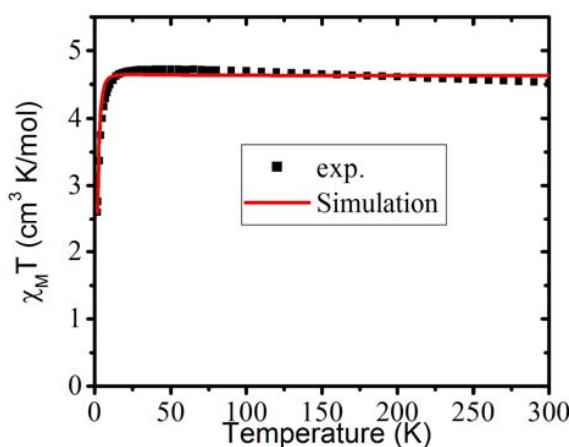


**Figure 8.** The magnetic  $\chi_M T$  vs.  $T$  plot of compound **1**, where the black squares are the experimental data, and the simulation based on Equation (1) is the red solid line.

#### 4. Conclusions

In conclusion, compound **1** can be considered as a “four-in-one” nonporous, supramolecular network, with its 3D entangled architecture being constructed via the inter-digitation of two crystallographically independent CPs forming porous (2D plus 2D) interdigitated double-layers, and then via the inter-penetration by two 1D crystallographically independent chain-like CPs, which displays an interesting moisture-sensitive induced colouring-changing property. Intra-CP and inter-CPs hydrogen bonding interaction and  $\pi$ - $\pi$  interactions among the four CPs play key roles in the stabilization of the 3D entangled architecture, showing high thermal-stability. Notably, an interesting reversible sponge-like water de-/ad-sorption behavior of **1** during the thermal re-/de-hydration processes, associated with colour-changing property and solid-state structural transformation between its de-hydrated and re-hydrated forms, is observed; this was successfully identified by cyclic TG analysis, and further demonstrated by PXRD measurements and morphological study. These thermally-induced, breathing-type dynamic effects suggest a reversible solid-state structural transformation of the entangled structure of **1** after water removal and retrieval from the pores, which is in agreement with the water-sorption studies, and could be attributed to the significant intra-/inter-CPs hydrogen bonding interactions and inter-CPs  $\pi$ - $\pi$  stacking interaction. This may be developed as a potential application of a thermally-induced moisture sensor. In this work, we successfully obtained a unique 3D-entangled supramolecular compound which displays interesting structural characteristics: reversible thermal-induced de-/re-hydration structural transformation associated with colour-changing behavior, magnetic property, and water hysteresis phenomenon in water vapor ad-/de-sorption isotherms. We thus believe that this nonporous composite entangled network should spark a broad spectrum of interest in the field of supramolecular chemistry.

**Supplementary Materials:** The following are available online at <http://www.mdpi.com/2073-4360/10/9/1014/s1>, Figure S1: The coordination environments of the Ni(II) ions in (a) [Ni(dpe)(Hbtc)(H<sub>2</sub>O)], **A**; (b) [Ni(dpe)(btc)(H<sub>2</sub>O)]<sup>−</sup>, **B**; (c) [Ni(dpe)(btc)(H<sub>2</sub>O)<sub>3</sub>]<sup>−</sup>, **C**; (d) [Ni(dpe)(H<sub>2</sub>O)<sub>4</sub>]<sup>2+</sup>, **D**. ORTEP drawing with 30% thermal ellipsoids. The solvated water molecules and H atoms are omitted for clarity, Table S1: Bond lengths (Å) around Ni(II) ions in **1**, Table S2: The related parameters of O–H...O hydrogen bonds for **1**, Table S3:  $\pi$ – $\pi$  interactions (face-to-face) in **1**.

**Author Contributions:** C.-C.W. conceived and designed the experiments; S.-Y.K., and K.-T.C. performed the experiments, including synthesis, structural characterization, EA, IR, TG analysis and water-absorption measurements of compound; M.-L.H., N.-K.S., and W.-F.L. contributed to measurements of luminescence property and analyzed the data; Y.-T.H., and B.-J.L. contributed to measurements of SEM of **1** and analyze the data; G.-H.L. contributed to the single-crystal X-ray Data collection and structural analysis; Y.-C.C. contributed to the powder X-ray diffraction measurements by synchrotron radiation light source; E.-C.Y., and S.-Y.H. contributed to analyze the magnetic data, including the fitting equation; C.-C.W., M.-L.H. and E.-C.Y. wrote the paper.

**Funding:** This research received no external funding.

**Acknowledgments:** The authors wish to thank the Ministry of Science and Technology, Taiwan and Soochow University for financial support.

**Conflicts of Interest:** The authors declare no conflict of interest.

## References

1. Batten, S.R.; Champness, N.R.; Chen, X.M.; Garcia-Martinez, J.; Kitagawa, S.; Öhrström, L.; O'keeffe, M.; Suh, M.P.; Reedijk, J. Terminology of metal–organic frameworks and coordination polymers. *Pure Appl. Chem.* **2013**, *85*, 1715–1724. [[CrossRef](#)]
2. Batten, S.R.; Champness, N.R.; Chen, X.M.; Garcia-Martinez, J.; Kitagawa, S.; Öhrström, L.; O'keeffe, M.; Suh, M.P.; Reedijk, J. Coordination polymers, metal–organic frameworks and the need for terminology guidelines. *CrystEngComm* **2012**, *14*, 3001–3004. [[CrossRef](#)]
3. O'Keeffe, M.; Peskov, M.A.; Ramsden, S.J.; Yaghi, O.M. The Reticular Chemistry Structure Resource (RCSR) Database of, and Symbols for, Crystal Nets. *Acc. Chem. Res.* **2008**, *41*, 1782–1789. [[CrossRef](#)] [[PubMed](#)]
4. Natarajan, S.; Mahata, P. Metal-organic framework structures—How closely are they related to classical inorganic structures? *Chem. Soc. Rev.* **2009**, *38*, 2304–2318. [[CrossRef](#)] [[PubMed](#)]
5. Blatov, V.A.; O'Keeffe, M.; Proserpio, D.M. Vertex-, face-, point-, Schläfli-, and Delaney-symbols in nets, polyhedra and tilings: Recommended terminology. *CrystEngComm* **2010**, *12*, 44–48. [[CrossRef](#)]
6. Alexandrov, E.V.; Blatov, V.A.; Kochetkov, A.V.; Proserpio, D.M. Underlying nets in three-periodic coordination polymers: Topology, taxonomy and prediction from a computer-aided analysis of the Cambridge Structural Database. *CrystEngComm* **2011**, *13*, 3947–3958. [[CrossRef](#)]
7. Baburin, I.A.; Blatov, V.A.; Carlucci, L.; Ciani, G.; Proserpio, D.M. Interpenetrated Three-Dimensional Networks of Hydrogen-Bonded Organic Species: A Systematic Analysis of the Cambridge Structural Database. *Cryst. Growth Des.* **2008**, *8*, 519–539. [[CrossRef](#)]
8. O'Keeffe, M.; Yaghi, O.M. Deconstructing the Crystal Structures of Metal–Organic Frameworks and Related Materials into Their Underlying Nets. *Chem. Rev.* **2012**, *112*, 675–702. [[CrossRef](#)] [[PubMed](#)]
9. Long, J.R.; Yaghi, O.M. The pervasive chemistry of metal–organic frameworks. *Chem. Soc. Rev.* **2009**, *38*, 1213–1314. [[CrossRef](#)] [[PubMed](#)]
10. Zhou, H.C.; Long, J.R.; Yaghi, O.M. Introduction to Metal–Organic Frameworks. *Chem. Rev.* **2012**, *112*, 673–674. [[CrossRef](#)] [[PubMed](#)]
11. Batten, S.R.; Neville, S.M.; Turner, D.R. *Coordination Polymers: Design, Analysis and Application*; Royal Society of Chemistry: Cambridge, UK, 2009.
12. Farrusseng, D. *Metal–Organic Frameworks Applications from Catalysis to Gas Storage*; Wiley: Weinheim, Germany, 2011.
13. Takamizawa, S.; Akatsuka, T.; Ueda, T. Gas-Conforming Transformability of an Ionic Single-Crystal Host Consisting of Discrete Charged Components. *Angew. Chem. Int. Ed.* **2008**, *47*, 1689–1692. [[CrossRef](#)] [[PubMed](#)]
14. Takamizawa, S.; Kohara, M.; Akatsuka, T.; Miyake, R. Gas-adsorbing ability of tris-ethylenediamine metal complexes (M = Co(III), Cr(III), Rh(III), Ir(III)) as transformable ionic single crystal hosts. *New J. Chem.* **2008**, *32*, 1782–1787. [[CrossRef](#)]



15. Morsali, A.; Masoomi, M.Y. Structures and properties of mercury(II) coordination polymers. *Coord. Chem. Rev.* **2009**, *253*, 1882–1905. [[CrossRef](#)]
16. Masoomi, M.Y.; Morsali, A. Applications of metal-organic coordination polymers as precursors for preparation of nano-materials Authors. *Coord. Chem. Rev.* **2012**, *256*, 2921–2943. [[CrossRef](#)]
17. Masoomi, M.Y.; Morsali, A. Morphological study and potential applications of nano metal-organic coordination polymer. *RSC Adv.* **2013**, *3*, 19191–19218. [[CrossRef](#)]
18. Aslani, A.; Morsali, A.; Zeller, M. Dynamic crystal-to-crystal conversion of a 3D–3D coordination polymer by de- and re-hydration. *Dalton Trans.* **2008**, 5173–5177. [[CrossRef](#)] [[PubMed](#)]
19. Pan, Q.H.; Li, J.Y.; Chen, Q.; Han, Y.D.; Chang, Z.; Song, W.C.; Bu, X.H. [Co(en)<sub>3</sub>]<sub>1/3</sub>[In(ox)<sub>2</sub>] · 3.5H<sub>2</sub>O: A zeolitic metal-organic framework templated by Co(en)<sub>3</sub>Cl<sub>3</sub>. *Microporous Mesoporous Mater.* **2010**, *132*, 453–457. [[CrossRef](#)]
20. Pan, Q.H.; Chen, Q.; Song, W.C.; Hu, T.L.; Bu, X.H. Template-directed synthesis of three new open-framework metal(II) oxalates using Co(III) complex as template. *CrystEngComm* **2010**, *12*, 4198–4204. [[CrossRef](#)]
21. Bertani, R.; Sgarbossa, P.; Venzo, A.; Lelj, F.; Amati, M.; Resnati, G.; Pilati, T.; Metrangolo, P.; Terraneo, G. Halogen bonding in metal-organic-supramolecular networks. *Coord. Chem. Rev.* **2010**, *254*, 677–695. [[CrossRef](#)]
22. Ingleson, M.J.; Bacsá, J.; Rosseinsky, M.J. Homochiral H-bonded proline based metal organic frameworks. *Chem. Commun.* **2007**, 3036–3038. [[CrossRef](#)] [[PubMed](#)]
23. Desiraju, G.R. C–H ··· O and other weak hydrogen bonds. From crystal engineering to virtual screening. *Chem. Commun.* **2005**, 2995–3001. [[CrossRef](#)] [[PubMed](#)]
24. García-Báez, E.V.; Martínez-Martínez, F.J.; Höpfl, H.; Padilla-Martínez, I.I.  $\pi$ -Stacking Interactions and CH···X (X = O, Aryl) Hydrogen Bonding as Directing Features of the Supramolecular Self-Association in 3-Carboxy and 3-Amido Coumarin Derivatives. *Cryst. Growth Des.* **2003**, *3*, 35–45. [[CrossRef](#)]
25. Janiak, C. A critical account on  $\pi$ – $\pi$  stacking in metal complexes with aromatic nitrogen-containing ligands. *Dalton Trans.* **2000**, 3885–3896. [[CrossRef](#)]
26. Claessens, C.G.; Stoddart, J.F.  $\pi$ – $\pi$  INTERACTIONS IN SELF-ASSEMBLY. *J. Phys. Org. Chem.* **1997**, *10*, 254–272. [[CrossRef](#)]
27. Guo, H.D.; Guo, X.M.; Batten, S.R.; Song, J.F.; Song, S.Y.; Dang, S.; Zhang, G.L.; Tang, J.K.; Zhang, H.J. Hydrothermal Synthesis, Structures, and Luminescent Properties of Seven d<sup>10</sup> Metal–Organic Frameworks Based on 9,9-Dipropylfluorene-2,7-Dicarboxylic Acid (H<sub>2</sub>DFDA). *Cryst. Growth Des.* **2009**, *9*, 1394–1401. [[CrossRef](#)]
28. Reger, D.L.; Horger, J.J.; Smith, M.D.; Long, G.J.; Grandjean, F. Homochiral, Helical Supramolecular Metal–Organic Frameworks Organized by Strong  $\pi$ ··· $\pi$  Stacking Interactions: Single-Crystal to Single-Crystal Transformations in Closely Packed Solids. *Inorg. Chem.* **2011**, *50*, 686–704. [[CrossRef](#)] [[PubMed](#)]
29. Fang, H.C.; Ge, Y.Y.; Jia, H.Y.; Li, S.S.; Sun, F.; Zhang, L.G.; Cai, Y.P. Construction of three high-dimensional supramolecular networks from temperature-driven conformational isomers. *CrystEngComm* **2011**, *13*, 67–71. [[CrossRef](#)]
30. Batten, S.R.; Hoskins, B.F.; Robson, R. Interdigitation, Interpenetration and Intercalation in Layered Cuprous Tricyanomethanide Derivatives. *Chem. Eur. J.* **2000**, *6*, 156–161. [[CrossRef](#)]
31. Batten, S.R.; Robson, R. Interpenetrating Nets: Ordered, Periodic Entanglement. *Angew. Chem. Int. Ed.* **1998**, *37*, 1460–1494. [[CrossRef](#)]
32. Wang, X.L.; Qin, C.; Wang, E.B.; Li, Y.G.; Su, Z.M.; Xu, L.; Carlucci, L. Entangled Coordination Networks with Inherent Features of Polycatenation, Polythreading, and Polyknotting. *Angew. Chem. Int. Ed.* **2005**, *44*, 5824–5827. [[CrossRef](#)] [[PubMed](#)]
33. Wu, H.; Liu, H.Y.; Liu, Y.Y.; Yang, J.; Liu, B.; Ma, J.F. An unprecedented 2D → 3D metal-organic polyrotaxane framework constructed from cadmium and a flexible star-like ligand. *Chem. Commun.* **2011**, *47*, 1818–1820. [[CrossRef](#)] [[PubMed](#)]
34. Baburin, I.A.; Blatov, V.A.; Carlucci, L.; Ciani, G.; Proserpio, D.M. Interpenetrating metal-organic and inorganic 3D networks: A computer-aided systematic investigation. Part II [1]. Analysis of the Inorganic Crystal Structure Database (ICSD). *J. Solid State Chem.* **2005**, *178*, 2452–2474. [[CrossRef](#)]
35. Carlucci, L.; Ciani, G.; Proserpio, D.M. Borromean links and other non-conventional links in ‘polycatenated’ coordination polymers: Re-examination of some puzzling networks. *CrystEngComm* **2003**, *5*, 269–279. [[CrossRef](#)]

36. Batten, S.R.; Harris, A.R.; Jensen, P.; Murray, K.S.; Ziebell, A. Copper(I) dicyanamide coordination polymers: Ladders, sheets, layers, diamond-like networks and unusual interpenetration. *J. Chem. Soc. Dalton Trans.* **2000**, 3829–3836. [[CrossRef](#)]
37. Chuang, Y.C.; Ho, W.L.; Sheu, C.F.; Lee, G.H.; Wang, Y. Crystal engineering from a 1D chain to a 3D coordination polymer accompanied by a dramatic change in magnetic properties. *Chem. Commun.* **2012**, *48*, 10769–10771. [[CrossRef](#)] [[PubMed](#)]
38. Zaman, M.B.; Smith, M.D.; Zur Loye, H.C. Two different one-dimensional structural motifs in the same coordination polymer: A novel interpenetration of infinite ladders by bundles of infinite chains. *Chem. Commun.* **2001**, 2256–2257. [[CrossRef](#)]
39. Mahmoudi, G.; Morsali, A. Novel rare case of 2D + 1D = 2D polycatenation Hg(II) coordination polymer. *CrystEngComm* **2009**, *11*, 50–51. [[CrossRef](#)]
40. Hagrman, D.; Hammond, R.P.; Haushalter, R.; Zubieta, J. Organic/Inorganic Composite Materials: Hydrothermal Syntheses and Structures of the One-, Two-, and Three-Dimensional Copper(II) Sulfate–Organodiamine Phases [Cu(H<sub>2</sub>O)<sub>3</sub>(4,4'-bipyridine)(SO<sub>4</sub>)]·2H<sub>2</sub>O, [Cu(bpe)<sub>2</sub>][Cu(bpe)(H<sub>2</sub>O)<sub>2</sub>(SO<sub>4</sub>)<sub>2</sub>]·2H<sub>2</sub>O, and [Cu(bpe)(H<sub>2</sub>O)(SO<sub>4</sub>)] (bpe = *trans*-1,2-Bis(4-pyridyl)ethylene). *Chem. Mater.* **1998**, *10*, 2091–2100.
41. Du, M.; Jiang, X.J.; Zhao, X.J. Direction of unusual mixed-ligand metal–organic frameworks: A new type of 3-D polythreading involving 1-D and 2-D structural motifs and a 2-fold interpenetrating porous network. *Chem. Commun.* **2005**, 5521–5523. [[CrossRef](#)] [[PubMed](#)]
42. Carlucci, L.; Ciani, G.; Moret, M.; Proserpio, D.M.; Rizzato, S. Polymeric Layers Catenated by Ribbons of Rings in a Three-Dimensional Self-Assembled Architecture: A Nanoporous Network with Spongelike Behavior. *Angew. Chem. Int. Ed.* **2000**, *39*, 1506–1510. [[CrossRef](#)]
43. Li, B.L.; Peng, Y.F.; Li, B.Z.; Zhang, Y. Supramolecular isomers in the same crystal: A new type of entanglement involving ribbons of rings and 2D (4,4) networks polycatenated in a 3D architecture. *Chem. Commun.* **2005**, 2333–2335. [[CrossRef](#)] [[PubMed](#)]
44. Biradha, K.; Fujita, M. A 'three-in-one' crystal of coordination networks. *Chem. Commun.* **2002**, 1866–1867. [[CrossRef](#)]
45. Wang, C.C.; Chung, W.C.; Lin, H.W.; Dai, S.C.; Shiu, J.S.; Lee, G.H.; Sheu, H.S.; Lee, W. Assembly of two Zinc(II)-sulfate coordination polymers with noncovalent and covalent bonds derived from flexible ligands, 1,2-bis(4-pyridyl)ethane (dpe). *CrystEngComm* **2011**, *13*, 2130–2136. [[CrossRef](#)]
46. Zheng, B.; Bai, J. An unprecedented nanoscale trilayered polythreading coordination array hierarchically formed from 2D square grid networks and induced by protonated 1,2-bis(4-pyridyl)ethane. *CrystEngComm* **2009**, *11*, 271–273. [[CrossRef](#)]
47. Carlucci, L.; Ciani, G.; Proserpio, D.M. Three-dimensional architectures of intertwined planar coordination polymers: The first case of interpenetration involving two different bidimensional polymeric motifs. *New J. Chem.* **1998**, *22*, 1319–1321. [[CrossRef](#)]
48. Shin, D.M.; Lee, I.S.; Chung, Y.K.; Lah, M.S. Coordination polymers based on square planar Co(II) node and linear spacer: Solvent-dependent pseudo-polymorphism and an unprecedented interpenetrating structure containing both 2D and 3D topological isomers. *Chem. Commun.* **2003**, 1036–1037. [[CrossRef](#)]
49. Ke, S.Y.; Chang, Y.F.; Wang, H.Y.; Yang, C.C.; Ni, C.W.; Lin, G.Y.; Chen, T.T.; Ho, M.L.; Lee, G.H.; Chuang, Y.C.; et al. Self-Assembly of Four Coordination Polymers in Three-Dimensional Entangled Architecture Showing Reversible Dynamic Solid-State Structural Transformation and Colour-Changing Behavior upon Thermal Dehydration and Rehydration. *Cryst. Growth Des.* **2014**, *8*, 4011–4018. [[CrossRef](#)]
50. Majumder, A.; Shit, S.; Choudhury, C.R.; Batten, S.R.; Pilet, G.; Luneau, D.; Daro, N.; Sutter, J.P.; Chattopadhyay, N.; Mitra, S. Synthesis, structure and fluorescence of two novel manganese(II) and zinc(II)-1,3,5-benzene tricarboxylate coordination polymers: Extended 3D supramolecular architectures stabilised by hydrogen bonding. *Inorg. Chim. Acta* **2005**, *358*, 3855–3864. [[CrossRef](#)]
51. Plater, M.J.; Foreman, M.R.; Coronado, E.; Gomez-Garcia, C.J.; Slawin, A.M.Z. Crystallisation of H<sub>3</sub>BTC, H<sub>3</sub>TPO or H<sub>2</sub>SDA with M<sup>II</sup> (M = Co, Mn or Zn) and 2,2'-bipyridyl: Design and control of co-ordination architecture, and magnetic properties (H<sub>3</sub>BTC = benzene-1,3,5-tricarboxylic acid, H<sub>3</sub>TPO = tris(4-carboxylphenyl)phosphine oxide, H<sub>2</sub>SDA = *cis*-stilbene-4,4'-dicarboxylic acid). *J. Chem. Soc. Dalton Trans.* **1999**, 4209–4216. [[CrossRef](#)]

52. Plater, M.J.; Foreman, M.R.; Howie, R.A.; Skakle, J.M.; Coronado, E.; Gómez-García, C.J.; Gelbrich, T.; Hursthouse, M.B. Synthesis and characterisation of polymeric metal-ion carboxylates from benzene-1,3,5-tricarboxylic acid with Mn(II), Co(II) or Zn(II) and 2,2-bipyridyl, phenanthroline or a pyridyl-2-(1-methyl-1H-pyrazol-3-yl) derivative. *Inorg. Chim. Acta* **2001**, *319*, 159–175. [[CrossRef](#)]
53. Du, M.; Jiang, X.J.; Zhao, X.J. Controllable Assembly of Metal-Directed Coordination Polymers under Diverse Conditions: A Case Study of the MII–H<sub>3</sub>tma/Bpt Mixed-Ligand System. *Inorg. Chem.* **2006**, *45*, 3998–4006. [[CrossRef](#)] [[PubMed](#)]
54. Jeong, S.; Kim, D.; Shin, S.; Moon, D.; Cho, S.J.; Lah, M.S. Combinational Synthetic Approaches for Isorecticular and Polymorphic Metal–Organic Frameworks with Tuned Pore Geometries and Surface Properties. *Chem. Mater.* **2014**, *26*, 1711–1719. [[CrossRef](#)]
55. Jeong, S.; Kim, D.; Song, X.; Choi, M.; Park, N.; Lah, M.S. Postsynthetic Exchanges of the Pillaring Ligand in Three-Dimensional Metal–Organic Frameworks. *Chem. Mater.* **2013**, *25*, 1047–1054. [[CrossRef](#)]
56. Hu, J.S.; Huang, L.F.; Yao, X.Q.; Qin, L.; Li, Y.Z.; Guo, Z.J.; Zheng, H.G.; Xue, Z.L. Six New Metal–Organic Frameworks Based on Polycarboxylate Acids and V-shaped Imidazole-Based Synthon: Syntheses, Crystal Structures, and Properties. *Inorg. Chem.* **2011**, *50*, 2404–2414. [[CrossRef](#)] [[PubMed](#)]
57. Gao, C.Y.; Liu, S.X.; Xie, L.H.; Sun, C.Y.; Cao, J.F.; Ren, Y.H.; Feng, D.; Su, Z.M. Rational design microporous pillared-layer frameworks: Syntheses, structures and gas sorption properties. *CrystEngComm* **2009**, *11*, 177–182. [[CrossRef](#)]
58. Gao, C.Y.; Liu, S.X.; Xie, L.H.; Ren, Y.H.; Cao, J.F.; Sun, C.Y. Design and construction of a microporous metal–organic framework based on the pillared-layer motif. *CrystEngComm* **2007**, *9*, 545–547. [[CrossRef](#)]
59. Prior, T.J.; Rosseinsky, M.J. A dense coordination polymer bearing an extensive and highly intricate hydrogen bonding array. *Chem. Commun.* **2001**, 1222–1223. [[CrossRef](#)]
60. Prior, T.J.; Rosseinsky, M.J. A porous one-dimensional coordination polymer composed of edge-shared hexagonal supramolecular units. *CrystEngComm* **2000**, *2*, 128–133. [[CrossRef](#)]
61. Wang, P.S.; Moorefield, C.N.; Panzer, M.; Newkome, G.R. Helical and polymeric nanostructures assembled from benzene tri- and tetracarboxylic acids associated with terpyridine copper(II) complexes. *Chem. Commun.* **2005**, 465–467. [[CrossRef](#)] [[PubMed](#)]
62. Pech, R.; Pickardt, J. catena-Triaqua- $\mu$ -[1,3,5-benzenetricarboxylato(2-)]-copper(II). *Acta Crystallogr. Sect. C Cryst. Struct. Commun.* **1988**, *44*, 992–994. [[CrossRef](#)]
63. Wang, Q.; Wu, M.J.; Wang, X.G.; Zhao, X.J. catena-Poly[[[aqua(5-amino-1H-1,2,4-triazole- $\kappa$ N<sup>4</sup>)zinc(II)]- $\mu$ -5-carboxy-benzene-1,3-dicarboxyl-ato] dihydrate]. *Acta Crystallogr.* **2006**, *62*, m2496–m2498.
64. Zhou, Y.F.; Lou, B.Y.; Yuan, D.Q.; Xu, Y.Q.; Jiang, F.L.; Hong, M.C. pH-value-controlled assembly of photoluminescent zinc coordination polymers. *Inorg. Chim. Acta* **2005**, *358*, 3057–3064. [[CrossRef](#)]
65. Yaghi, O.M.; Li, G.M.; Li, H.L. Crystal Growth of Extended Solids by Nonaqueous Gel Diffusion. *Chem. Mater.* **1997**, *9*, 1074–1076. [[CrossRef](#)]
66. Shi, X.; Zhu, G.S.; Fang, Q.R.; Wu, G.; Tian, G.; Wang, R.W.; Zhang, D.L.; Xue, M.; Qiu, S.L. Novel Supramolecular Frameworks Self-Assembled from One-Dimensional Polymeric Coordination Chains. *Eur. J. Inorg. Chem.* **2004**, *2004*, 185–191. [[CrossRef](#)]
67. Riou-Cavellec, M.; Albinet, C.; Greneche, J.M.; Ferey, G. Study of the iron/trimesic acid system for the hydrothermal synthesis of hybrid materials. *J. Mater. Chem.* **2001**, *11*, 3166–3171. [[CrossRef](#)]
68. Ding, B.B.; Weng, Y.Q.; Mao, Z.W.; Lam, C.K.; Chen, X.M.; Ye, B.H. Pillared-Layer Microporous Metal–Organic Frameworks Constructed by Robust Hydrogen Bonds. Synthesis, Characterization, and Magnetic and Adsorption Properties of 2,2'-Biimidazole and Carboxylate Complexes. *Inorg. Chem.* **2005**, *44*, 8836–8845. [[CrossRef](#)] [[PubMed](#)]
69. Yaghi, O.M.; Li, H.L.; Groy, T.L. Construction of Porous Solids from Hydrogen-Bonded Metal Complexes of 1,3,5-Benzenetricarboxylic Acid. *J. Am. Chem. Soc.* **1996**, *118*, 9096–9101. [[CrossRef](#)]
70. Yaghi, O.M.; Li, G.; Li, H.L. Selective binding and removal of guests in a microporous metal–organic framework. *Nature* **1995**, *378*, 703–706. [[CrossRef](#)]
71. Daiguebonne, C.; Deluzet, A.; Camara, M.; Boubekeur, K.; Audebrand, N.; Gerault, Y.; Baux, C.; Guillou, O. Lanthanide-Based Molecular Materials: Gel Medium Induced Polymorphism. *Cryst. Growth Des.* **2003**, *3*, 1015–1020. [[CrossRef](#)]
72. Choi, K.Y.; Chun, K.M.; Suh, I.H. Synthesis and characterization of one-dimensional nickel(II) macrocyclic complexes with bridging organic ligands. *Polyhedron* **2001**, *20*, 57–65. [[CrossRef](#)]

73. Wang, X.; Le, M.; Lin, H.Y.; Luan, J.; Liu, G.C.; Sui, F.F.; Chang, Z.H. Assembly, structures, photophysical properties and photocatalytic activities of a series of coordination polymers constructed from semi-rigid bis-pyridyl-bis-amide and benzenetricarboxylic acid. *Inorg. Chem. Front.* **2015**, *2*, 373–387. [[CrossRef](#)]
74. Tomar, K.; Rajak, R.; Sanda, S.; Konar, S. Synthesis and Characterization of Polyhedral-Based Metal–Organic Frameworks Using a Flexible Bipyrazole Ligand: Topological Analysis and Sorption Property Studies. *Cryst. Growth Des.* **2015**, *15*, 2732–2741. [[CrossRef](#)]
75. Habib, H.A.; Sanchiz, J.; Janiak, C. Mixed-ligand coordination polymers from 1,2-bis(1,2,4-triazol-4-yl)ethane and benzene-1,3,5-tricarboxylate: Trinuclear nickel or zinc secondary building units for three-dimensional networks with crystal-to-crystal transformation upon dehydration. *Dalton Trans.* **2008**, 1734–1744. [[CrossRef](#)] [[PubMed](#)]
76. Bradshaw, P.; Prior, T.J.; Cussen, E.J.; Claridge, J.B.; Rosseinsky, M.J. Permanent Microporosity and Enantioselective Sorption in a Chiral Open Framework. *J. Am. Chem. Soc.* **2004**, *126*, 6106–6114. [[CrossRef](#)] [[PubMed](#)]
77. Zhao, X.; Xiao, B.; Fletcher, A.J.; Thomas, K.M.; Bradshaw, D.; Rosseinsky, M.J. Hysteretic adsorption and desorption of hydrogen by nanoporous metal-organic frameworks. *Science* **2004**, *306*, 1012–1015. [[CrossRef](#)] [[PubMed](#)]
78. Prior, T.J.; Bradshaw, D.; Teat, S.J.; Rosseinsky, M.J. Designed layer assembly: A three-dimensional framework with 74% extra-framework volume by connection of infinite two-dimensional sheets. *Chem. Commun.* **2003**, 500–501. [[CrossRef](#)]
79. Lu, T.B.; Xiang, H.; Luck, R.L.; Jiang, L.; Mao, Z.W.; Ji, L.N.  $[\text{NiL}]_3[\text{BTC}]_2 \cdot 14\text{H}_2\text{O}$  [L = 3,10-bis(2-ethyl)-1,3,5,8,10,12-hexaazacyclotetradecane, BTC = 1,3,5-benzenetricarboxylate]: Synthesis, structure and unique selective guest molecule absorption properties. *New J. Chem.* **2002**, *26*, 969–971. [[CrossRef](#)]
80. Lu, T.B.; Xiang, H.; Luck, R.L.; Mao, Z.W.; Wang, D.; Chen, C.; Ji, L.N. A two-dimensional coordination polymer with a brick wall structure and hydrophobic channels: Synthesis and structure of a macrocyclic nickel(II) complex with 1,3,5-benzenetricarboxylate. *CrystEngComm* **2001**, *3*, 168–169. [[CrossRef](#)]
81. Kepert, C.J.; Prior, T.J.; Rosseinsky, M.J. A Versatile Family of Interconvertible Microporous Chiral Molecular Frameworks: The First Example of Ligand Control of Network Chirality. *J. Am. Chem. Soc.* **2000**, *122*, 5158–5168. [[CrossRef](#)]
82. Kepert, C.J.; Rosseinsky, M.J. A porous chiral framework of coordinated 1,3,5-benzenetricarboxylate: Quadruple interpenetration of the (10,3)-a network. *Chem. Commun.* **1998**, 31–32. [[CrossRef](#)]
83. Choi, H.J.; Suh, M.P. Self-Assembly of Molecular Brick Wall and Molecular Honeycomb from Nickel(II) Macrocyclic and 1,3,5-Benzenetricarboxylate: Guest-Dependent Host Structures. *J. Am. Chem. Soc.* **1998**, *120*, 10622–10628. [[CrossRef](#)]
84. Holmes, K.E.; Kelly, P.F.; Elsegood, M.R.J. Honeycombs, herringbones and brick-walls; three-fold guest-dependent variation in copper trimesate complexes bearing sulfimide ligands. *Dalton Trans.* **2004**, 3488–3494. [[CrossRef](#)] [[PubMed](#)]
85. Ko, J.W.; Min, K.S.; Suh, M.P. A Hybrid Consisting of Coordination Polymer and Noncovalent Organic Networks: A Highly Ordered 2-D Phenol Network Assembled by Edge-to-Face  $\pi$ - $\pi$  Interactions. *Inorg. Chem.* **2002**, *41*, 2151–2157. [[CrossRef](#)] [[PubMed](#)]
86. Oshio, H.; Ichida, H. Control of Intramolecular Magnetic Interaction by the Spin Polarization of d.p.i. Spin to p.p.i. Orbital of an Organic Bridging Ligand Hiroki Oshio, and Hikaru Ichida. *J. Phys. Chem.* **1995**, *99*, 3294–3302. [[CrossRef](#)]
87. Zhang, J.; Chen, Y.B.; Chen, S.M.; Li, Z.J.; Cheng, J.K.; Yao, Y.G. A Polar Luminescent Zn Polymer Containing an Unusual Noninterpenetrated utp Net. *Inorg. Chem.* **2006**, *45*, 3161–3163. [[CrossRef](#)] [[PubMed](#)]
88. Wu, G.; Shi, X.; Fang, Q.R.; Tian, G.; Wang, L.F.; Zhu, G.S.; Addison, A.W.; Wei, Y.; Qiu, S.L. Triethylammonium benzene-1,3,5-tricarboxylate(pyridine)zinc(II): A two-dimensional undulating mesh network. *Inorg. Chem. Commun.* **2003**, *6*, 402–404. [[CrossRef](#)]
89. Li, X.J.; Sun, D.F.; Cao, R.; Sun, Y.Q.; Wang, Y.Q.; Bi, W.H.; Gao, S.Y.; Hong, M.C.  $[\text{Zn}_2(\text{H}_2\text{O})_3(2,2'\text{-bipy})_2(\text{btc})][\text{Zn}(\text{H}_2\text{O})(2,2'\text{-bipy})(\text{btc})] \cdot 8\text{H}_2\text{O}$ : A novel zinc-carboxylate complex consisting of independently cationic and anionic chains. *Inorg. Chem. Commun.* **2003**, *6*, 908–911. [[CrossRef](#)]
90. Smith, G.; Reddy, A.N.; Byriel, K.A.; Kennard, C.H.L. Preparation and crystal structures of the silver(I) carboxylates  $[\text{Ag}_2\{\text{C}_6\text{H}_4(\text{CO}_2)_2\}(\text{NH}_3)_2]$ ,  $[\text{NH}_4][\text{Ag}_5\{\text{C}_6\text{H}_3(\text{CO}_2)_3\}_2(\text{NH}_3)_2(\text{H}_2\text{O})_2] \cdot \text{H}_2\text{O}$  and  $[\text{NH}_4][\text{Ag}\{\text{C}_4\text{H}_2\text{N}_2(\text{CO}_2)_2\}]$ . *J. Chem. Soc. Dalton Trans.* **1995**, 3565–3570. [[CrossRef](#)]



91. Gomez-Lor, B.; Gutierrez-Puebla, E.; Iglesias, M.; Monge, M.A.; Ruiz-Valero, C.; Snejko, N. Novel 2D and 3D Indium Metal-Organic Frameworks: Topology and Catalytic Properties. *Chem. Mater.* **2005**, *17*, 2568–2573. [[CrossRef](#)]
92. SMART V 4.043 Software for CCD Detector System; Siemens Analytical Instruments Division: Madison, WI, USA, 1995.
93. SAINT V 4.035 Software for CCD Detector System; Siemens Analytical Instruments Division: Madison, WI, USA, 1995.
94. Sheldrick, G.M. *Program for the Refinement of Crystal Structures*; University of Göttingen: Göttingen, Germany, 1993.
95. SHELXTL 5.03 (PC-Version), *Program Library for Structure Solution and Molecular Graphics*; Siemens Analytical Instruments Division: Madison, WI, USA, 1995.
96. Hammersley, A.P.; Svensson, S.O.; Hanfland, M.; Fitch, A.N.; Häusermann, D. Two-dimensional detector software: From real detector to idealised image or two-theta scan. *High Press. Res.* **1996**, *14*, 235–248. [[CrossRef](#)]
97. Wang, C.C.; Yang, C.C.; Yeh, C.T.; Cheng, K.Y.; Chang, P.C.; Ho, M.L.; Lee, G.H.; Shih, W.J.; Sheu, H.S. Reversible Solid-State Structural Transformation of a 1D–2D Coordination Polymer by Thermal De/Rehydration Processes. *Inorg. Chem.* **2011**, *50*, 597–603. [[CrossRef](#)] [[PubMed](#)]
98. Qin, L.; Wang, Z.J.; Wang, T.; Zheng, H.G.; Chen, J.X. Coligand-directed synthesis of five Co(II)/Ni(II) coordination polymers with a neutral tetradentate ligand: Syntheses, crystal structures, and properties. *Dalton Trans.* **2014**, *43*, 12528–12535. [[CrossRef](#)] [[PubMed](#)]
99. Taşdemir, E.; Özbek, F.E.; Sertçelik, M.; Hökelek, T.; Çelik, R.Ç.; Necefoğlu, H. Supramolecular complexes of Co(II), Ni(II) and Zn(II) p-hydroxybenzoates with caffeine: Synthesis, spectral characterization and crystal structure. *J. Mol. Struct.* **2016**, *1119*, 472–478. [[CrossRef](#)]
100. Kharadi, G.J. Thermal and Microbicidal Study of Coordination Polymers: Transition Metal with 8HQMIT Ligand. *Synth. React. Inorg. Met.-Org. Nano-Met. Chem.* **2014**, *44*, 1001–1010. [[CrossRef](#)]
101. Borrás-Almenar, J.J.; Clemente-Juan, J.M.; Coronado, E.; Tsukerblat, B.S. High-nuclearity magnetic clusters: generalized spin Hamiltonian and its use for the calculation of the energy levels, bulk magnetic properties, and inelastic neutron scattering spectra. *Inorg. Chem.* **1999**, *38*, 6081–6088. [[CrossRef](#)] [[PubMed](#)]
102. Borrás-Almenar, J.J.; Clemente-Juan, J.M.; Coronado, E.; Tsukerblat, B.S. MAGPACK<sup>1</sup> A package to calculate the energy levels, bulk magnetic properties, and inelastic neutron scattering spectra of high nuclearity spin clusters. *J. Comput. Chem.* **2001**, *22*, 985–991. [[CrossRef](#)]
103. Shin, J.W.; Kim, D.W.; Moon, D. Syntheses and characterization of various supramolecular compounds from the self-assembly of nickel (II) hexaaza macrocyclic complex with carboxylic acid derivatives. *Polyhedron* **2016**, *105*, 62–70. [[CrossRef](#)]
104. Bi, J.H.; Li, M.; Yao, Z.L. Synthesis and Magnetic Properties of [Ni<sub>3</sub>(BTC)<sub>2</sub>(H<sub>2</sub>O)<sub>12</sub>] n (BTC= 1, 3, 5-Benzenetricarboxylate). *Asian J. Chem.* **2011**, *23*, 5181.
105. Cortijo, M.; Herrero, S.; Jiménez-Aparicio, R.; Matesanz, E. Modulation of the Magnetic Properties of Two-Dimensional Compounds [NiX<sub>2</sub> (N–N)] by Tailoring Their Crystal Structure. *Inorg. Chem.* **2013**, *52*, 7087–7093. [[CrossRef](#)] [[PubMed](#)]



© 2018 by the authors. Licensee MDPI, Basel, Switzerland. This article is an open access article distributed under the terms and conditions of the Creative Commons Attribution (CC BY) license (<http://creativecommons.org/licenses/by/4.0/>).